Probing the fusion of ^{7}Li with ^{64}Ni at near-barrier energies

Md. Moin Shaikh,[1] Subinit Roy,[1,*] S. Rajbanshi,[1] A. Mukherjee,[1] M. K. Pradhan,[1] P. Basu,[1] V. Nanal,[2] S. Pal,[2] A. Shrivastava,[3] S. Saha,[2] and R. G. Pillay[2]

[1]*Nuclear Physics Division, Saha Institute of Nuclear Physics, Kolkata 700 064, India*

[2]*Department of Nuclear and Atomic Physics, Tata Institute of Fundamental Research, Mumbai 400 005, India*

[3]*Nuclear Physics Division, Bhabha Atomic Research Centre, Mumbai 400 085, India*

(Received 22 February 2016; published 25 April 2016)

Background: The stable isotopes of Li, ^{6}Li and ^{7}Li, have two-body cluster structures of $\alpha + d$ and $\alpha + t$ with α-separation energies or *breakup thresholds* at 1.47 and 2.47 MeV, respectively. The weak binding of these projectiles introduces several new reaction channels not usually observed in the case of strongly bound projectiles. The impact of these breakup or breakup-like reaction channels on fusion, the dominant reaction process at near-barrier energies, with different target masses is of current interest.

Purpose: Our purpose is to explore the fusion, at above and below the Coulmb barrier, of ^{7}Li with ^{64}Ni target in order to understand the effect of breakup or breakup-like processes with medium-mass target in comparison with ^{6}Li, which has a lower breakup threshold.

Measurement: The total fusion (TF) excitation of the weakly bound projectile ^{7}Li with the medium-mass target ^{64}Ni has been measured at the near-barrier energies (0.8 to 2 V_B). The measurement was performed using the online characteristic γ-ray detection method. The complete fusion (CF) excitation function for the system was obtained using the xn-evaporation channels with the help of statistical model predictions.

Results: At the above barrier energies CF cross sections exhibit an average suppression of about 6.5% compared to the one-dimensional barrier penetration model (1DBPM) predictions, while the model describes the measured TF cross section well. But below the barrier, both TF and CF show enhancements compared to 1DBPM predictions. Unlike ^{6}Li, enhancement of CF for ^{7}Li could not be explained by inelastic coupling alone.

Conclusion: Whereas the $\sigma_{\rm TF}$ cross sections are almost the same for both the systems in the above barrier region, the suppression of $\sigma_{\rm CF}$ at above the barrier is less for the ^{7}Li $+^{64}$Ni system than for the ^{6}Li $+^{64}$Ni system. Also direct cluster transfer has been identified as the probable source for producing large enhancement in TF cross sections.

DOI: 10.1103/PhysRevC.93.044616

I. INTRODUCTION

Understanding the effect of breakup or breakup-like reactions, with three-body final states, on fusion is an important goal of recent studies of heavy-ion collisions with weakly bound projectiles around the Coulomb-barrier energies [1,2]. The weak binding property, i.e., the breakup of the weakly bound nuclei into their cluster components, opens up many new processes like sequential complete fusion (SCF) of all the fragments after breakup. The residues produced with this method are the same as those produced with the direct complete fusion (DCF) process of the whole projectile. Therefore the measured complete fusion (CF = DCF + SCF) is the sum of the two. The capture of a part of the projectile after its breakup by the target leads to incomplete fusion (ICF). The sum of CF and ICF is measured as total fusion (TF). The TF and CF cross sections are experimentally distinguishable in collisions of weakly bound projectiles with heavy-mass targets [3–8]. The CF cross sections in the above-barrier region are found to be suppressed compared to the measured TF cross sections, which are well described by theoretical models. The suppression of CF cross sections, consequently, is attributed to lost flux, which went to ICF channels [9]. On the other hand, in the below-barrier region both the TF and CF cross sections are enhanced compared to the 1DBPM prediction.

In the case of lower-mass targets, the charge particle evaporation channels become dominant, making the CF and ICF channels indistinguishable. Hence, the measurement provides only the TF cross sections [10–16]. However, to investigate the variation of the degree of suppression of CF cross sections at above-barrier energies with the decrease of target charge and mass as well as to understand the fusion enhancements in the below-barrier region, it is necessary to obtain the CF cross sections for these systems.

In a recent work by our group on the ^{6}Li $+^{64}$Ni system [12], detailed measurement of the fusion excitation function has been reported and $\sigma_{\rm CF}$ is extracted from the measured $\sigma_{\rm TF}$ with the help of a statistical model. The results indicate that CF cross sections are suppressed by an average suppression of about 13% compared to the TF cross sections in the above-barrier region, which are well described by 1DBPM and coupled-channels calculations. In the below-barrier region, both CF and TF cross sections are enhanced compared to 1DBPM predictions. While the CF enhancement could be explained using the channel coupling to inelastic excitations, the origin of observed enhancement of $\sigma_{\rm TF}$ in the same energy region could not be clearly understood.

The scenario is further investigated in the present work for the fusion of ^{7}Li, the other stable Li isotope with the same

*subinit.roy@saha.ac.in

TABLE I. The observed characteristic γ-ray transitions of different residues to their corresponding ground states. The spin-parity of the state 237.8 (*) of ^{66}Cu is unknown [18,19].

Residue channel	Transitions Excited state (J^π) $\rightarrow$ ground state (J^π)	E_γ (keV)
	$1/2^- \rightarrow 3/2^-$	318.7
	$5/2^- \rightarrow 3/2^-$	574.2
^{69}Ga	$3/2^- \rightarrow 3/2^-$	872.1
($2n$)	$5/2^- \rightarrow 3/2^-$	1106.9
	$7/2^- \rightarrow 3/2^-$	1336.4
	$7/2^- \rightarrow 3/2^-$	1488.0
^{69}Zn	$9/2^+ \rightarrow 1/2^-$	438.6
(pn)	$3/2^- \rightarrow 1/2^-$	834.5
	$2^+ \rightarrow 1^+$	175.0
	$1^+ \rightarrow 1^+$	321.0
^{68}Ga	$2^+ \rightarrow 1^+$	374.6
($3n$)	$(0,1,2)^+ \rightarrow 1^+$	555.5
	$2^+ \rightarrow 1^+$	564.5
	$2^- \rightarrow 1^+$	583.8
	$1^+, 2^+ \rightarrow 1^+$	825.3
^{68}Zn ($p2n$)	$2^+ \rightarrow 0^+$	1077.4
	$2^+ \rightarrow 1^+$	185.95
^{66}Cu	$(\leqslant 3^+)^* \rightarrow 1^+$	237.8
(αn)	$1^+ \rightarrow 1^+$	385.8
	$2^+ \rightarrow 1^+$	465.2
	$1^+ \rightarrow 1^+$	1052.1
	$1/2^- \rightarrow 3/2^-$	770.6
^{65}Cu	$5/2^- \rightarrow 3/2^-$	1115.6
($\alpha 2n$)	$7/2^- \rightarrow 3/2^-$	1481.8

^{64}Ni target. The nucleus ^{7}Li with an α-separation energy of 2.47 MeV has a bound excited state at 0.478 MeV ($1/2^-$) and is deformed. Hence, it is important to explore the fusion of ^{7}Li with the ^{64}Ni target in order to understand the effect of breakup or breakup-like processes with medium-mass targets in comparison with ^{6}Li.

II. EXPERIMENTAL DETAILS

The experiment was performed at the Pelletron Linac Facility in Mumbai, India. The experimental setup was almost similar to that used in the ^{6}Li + ^{64}Ni fusion measurement and described in Ref. [12]. The choice of ^{64}Ni ($N/Z = 1.28$) as the target was prompted by the presence of eight valence neutrons over the closed $N = 28$ subshell compared to two in ^{58}Ni ($N/Z = 1.07$). The compound nucleus with the ^{64}Ni target decays predominantly through xn-evaporation channels, which favors the extraction of the CF cross section from the measured yield. The ^{7}Li beam with energy from 12 to 28 MeV was bombarded on a self-supporting 507 ± 10 μg/cm^2 thick metallic ^{64}Ni target (~99% enriched) in small energy steps. The energy steps were 0.5 MeV from 12 to 15 MeV, 1 MeV from 15 to 20 MeV, and 2 MeV at higher energies. The background spectra were recorded after each energy run. A high-purity germanium (HPGe) detector of energy resolution

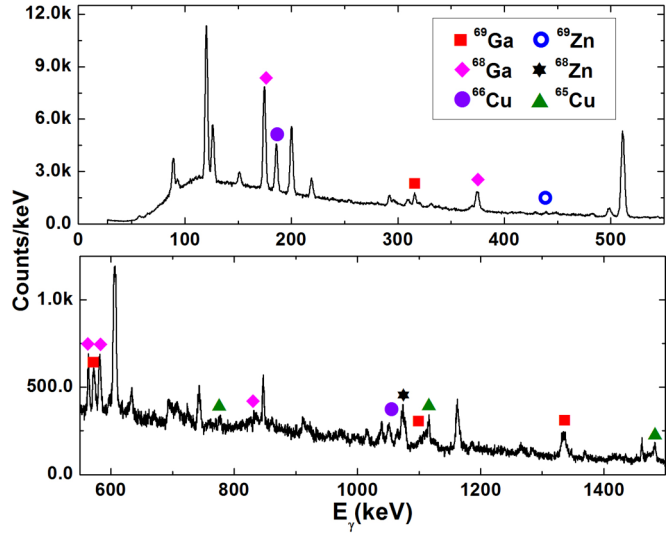

FIG. 1. Representative characteristic γ-ray spectrum from the collision of the system ^{7}Li + ^{64}Ni at $E_{\rm lab} = 24$ MeV. Some of the characteristic γ transitions of the residues are marked.

2.8 keV at the 1408-keV γ line of ^{152}Eu was positioned at 135° with respect to the beam direction. This detector was used to detect the γ rays emitted from the residues. The absolute efficiency (ϵ_γ) of the detector was determined by using calibrated radioactive sources of ^{152}Eu and ^{133}Ba at the target position. The data were recorded and analyzed using the CAMAC-based multiparameter acquisition system LAMPS [17].

The observed γ rays from the residues produced from the fusion of ^{7}Li with ^{64}Ni are shown in Table I and a representative characteristic γ-ray spectrum at $E_{\rm lab} = 24$ MeV is shown in Fig. 1.

Offline measurement

The major drawback of the online characteristic γ-ray method is that it cannot measure the direct ground-state populations of the residues. To estimate the direct ground-state feeding an offline measurement has been performed using the detection of characteristic x rays after the unstable residue ^{68}Ga ($T_{1/2} = 67.7$ min) decays to the daughter nucleus ^{68}Zn through the electron capture process. For the offline analysis a separate run with the ^{7}Li beam of energy 26 MeV was taken using a fresh ^{64}Ni target of same thickness. A gold catcher foil of thickness 4 mg/cm^2 was placed behind the target to stop the recoiling residues. Immediately after the irradiation the target arrangement was taken out from the reaction chamber and was mounted in front of the x-ray detector for offline measurement. The branching ratio of the decay of ^{68}Ga to the ground state of ^{68}Zn is 97% [18]. The delayed x rays, characteristic of Zn, emitted in the process were recorded. A standard ^{241}Am x-ray source was used to determine the efficiency of the x-ray detector. The necessary parameters like relative intensities, fluorescence yields of relevant K x rays, etc., were taken from Ref. [20]. The ^{68}Ga residue can only be produced from the complete fusion of ^{7}Li and ^{64}Ni. Offline x-ray measurement gives the cross section of formation of ^{68}Ga including the

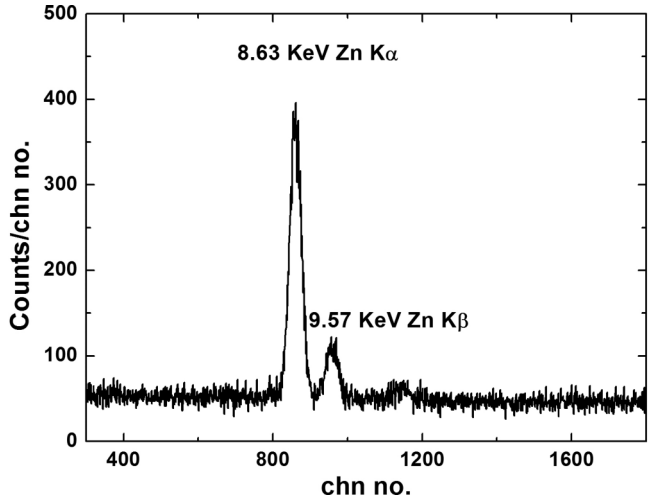

FIG. 2. Representative characteristic offline x-ray spectrum from the fusion of the system ^{7}Li + ^{64}Ni at $E_{\rm lab} = 26$ MeV. The characteristic K x-rays of Zn have been marked.

direct ground-state population. A typical offline characteristic delayed x-ray spectrum following ^{7}Li and ^{64}Ni collision at 26 MeV is shown in Fig. 2.

The experimental data and corresponding fitted growth curve, $Y(t)(= Y(0)[1 - \exp(0.693t/T_{1/2})])$, of the daughter nucleus ^{68}Zn is shown in Fig. 3. The resulting half-life of the parent nucleus ^{68}Ga from the fitted curve is 65.7± 2.0 min, which is very close to the value (67.7 min) available in the literature. The extrapolation of the curve yields the number of ^{68}Ga nuclei present at the start ($t = 0$) of the offline acquisition. The final yield of ^{68}Ga is extracted using the measured half-life and taking into account the decay during irradiation. The resultant residue cross section is obtained by incorporating the corrections for fluorescence and branching factor. The derived residue cross section at 26 MeV that

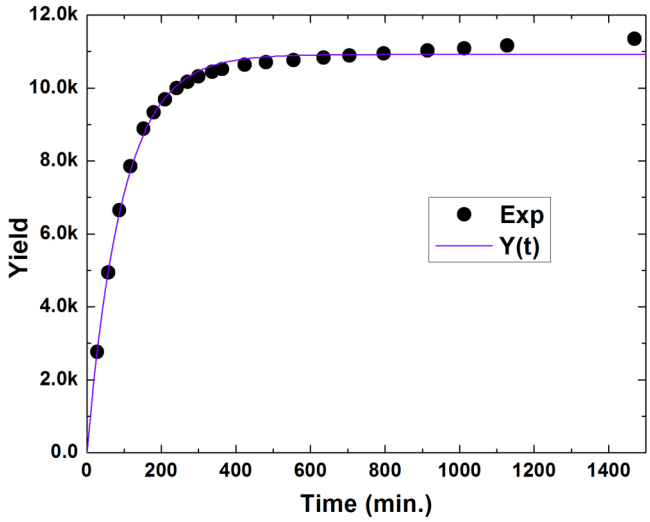

FIG. 3. The experimental data and the fitted growth curve, $Y(t)$, as a function of time of the daughter nuclei (Zn) of ^{68}Ga from offline measurement of the system ^{7}Li + ^{64}Ni.

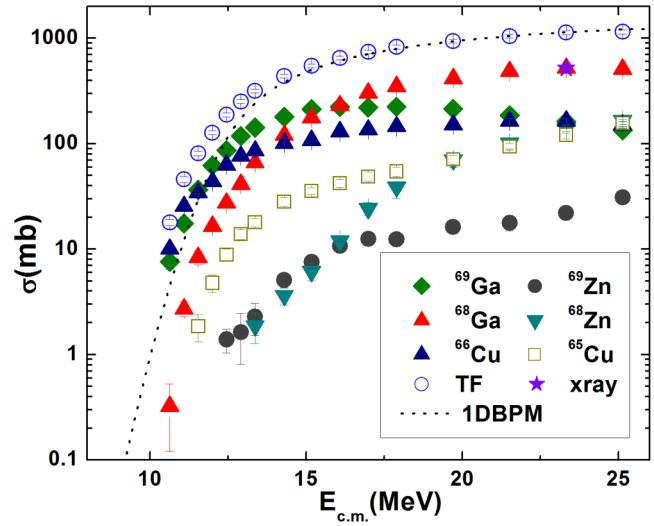

FIG. 4. The measured excitation functions of individual residue channels are shown along with the experimental TF excitation function for the system ^{7}Li + ^{64}Ni. The dotted line represents the 1DBPM prediction for fusion. The cross section of the residue ^{68}Ga for $E_{\rm lab} = 26$ MeV from offline x-ray measurement is shown by a solid star.

includes the direct ground-state feeding component, if any, is shown in Fig. 4. The cross section matches nicely with the cross section of ^{68}Ga estimated from online characteristic γ-ray measurements. This supports the conjecture that direct particle feeding to the ground state of the residues in this mass and energy region is not significant [12,21,22].

III. ANALYSIS AND RESULTS

A. Excitation function of fusion channels

The compound nucleus ^{71}Ga, produced in the collision of the system ^{7}Li + ^{64}Ni, predominantly decays through the $2n$- and $3n$-evaporation channels. The evaporation residues from decay channels pn, $p2n$ and/or t, αn, and $\alpha 2n$ are also observed. The residues produced through $2n$-, $3n$-, and pn-evaporation channels are associated only with the CF process. The other channels are produced from the CF process as well as from other processes like fusion following breakup or transfer-breakup reactions. As an example the residue produced from the CF process through the αn channel can also be produced from the t-ICF process with subsequent evaporation of a neutron. The direct cluster transfer (DCT) to the unbound state of ^{67}Cu can also populate the channel.

Each evaporation residue channel cross section ($\sigma_{\rm chn}^{\rm exp}$) is obtained by summing over the measured cross sections of the observed γ-ray transitions directly to the ground state of the residue. The experimental TF cross section ($\sigma_{\rm TF}^{\rm exp}$) at each energy is obtained from

$$\sigma_{\rm TF}^{\rm exp} = \sum_{\rm chn} \sigma_{\rm chn}^{\rm exp}. \quad (1)$$

Table I shows the dominant direct γ-ray transitions from the excited states to the ground state of the residues, which

TABLE II. Q values of different reaction channels for the ^{7}Li and ^{64}Ni projectile-target system.

Reaction channel	Q_{gg} (MeV)
^{64}Ni(^{7}Li ,^{8}Li)^{63}Ni	−7.623
^{64}Ni(^{7}Li ,^{6}Li)^{65}Ni	−1.153
^{64}Ni(^{7}Li ,^{6}He)^{65}Cu	−2.520
^{64}Ni(^{7}Li ,^{5}He)^{66}Cu	2.835
^{64}Ni(^{7}Li ,^{4}He)^{67}Cu	12.703
^{64}Ni(^{7}Li ,^{3}H)^{68}Zn	2.866
^{64}Ni(^{7}Li ,^{1}H)^{70}Zn	10.084

have been used to estimate the residue or channel cross sections.

The estimated cross sections do not include the contributions of direct ground-state feeding of the residues, an inherent limitation of characteristic γ-ray measurement. However, it has been shown that in this mass region the direct ground-state feeding is negligible [12], which is verified also by our offline measurements.

The measured excitation functions of individual residues and $\sigma_{\rm TF}^{\rm exp}$ are shown in Fig. 4. The Q-values of relevant reaction channels are given in Table II. The residues ^{66}Cu and ^{65}Cu, shown in Fig. 4, have mixed origins. The residue ^{66}Cu has many sources like CF, t-ICF, and t-stripping to neutron unbound states of the ^{67}Cu owing to the large positive Q value. It can also be produced by deuteron transfer from the projectile ^{7}Li to the target ^{64}Ni. On the other hand ^{65}Cu can be produced from CF, t-ICF, and one-proton stripping processes.

B. Extraction of complete fusion

In order to estimate the suppression, if any, of the CF cross section of ^{7}Li with ^{64}Ni at above-barrier energies, we attempted to extract the CF cross section from the measured channel cross sections. The CF cross sections have been estimated from the two most dominating pure complete fusion channels, the $2n$ and $3n$ channels, by taking help from the statistical model (SM) code PACE4 [23]. Over the incident energy range of 28 MeV to 12 MeV, the summed model cross sections of the $2n$ and $3n$ channels constitute about 62% to 87%, respectively. The summed cross sections of these two channels from experimental data, $\sigma_{2n+3n}^{\rm exp}$, and from SM predictions, $\sigma_{2n+3n}^{\rm stat}$, are plotted in Fig. 5. It is clear from Fig. 5 that the summed experimental cross sections for the $2n$- and $3n$-evaporation channels agree well with the SM predictions over the whole energy range. The branching ratio from the SM calculations for these two channels to the model CF, $R_{\rm CF}^{2n+3n}$, is defined as

$$R_{\rm CF}^{2n+3n} = \frac{\sigma_{\rm CF}^{\rm stat}}{\sigma_{2n+3n}^{\rm stat}}. \quad (2)$$

Therefore, the CF cross section, $\sigma_{\rm CF}$, can be obtained from the measured summed cross section of $2n$ and $3n$ channels by using the relation

$$\sigma_{\rm CF} = \frac{\sigma_{2n+3n}^{\rm exp}}{R_{\rm CF}^{2n+3n}}. \quad (3)$$

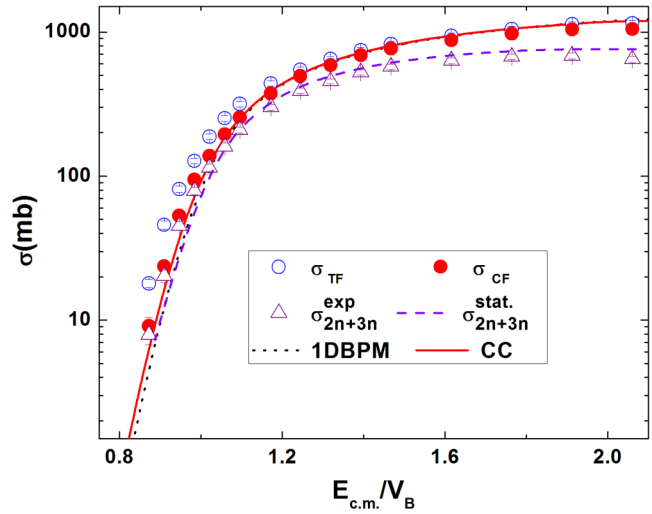

FIG. 5. The measured TF (open bullet), derived CF (solid bullet), and experimental $(2n + 3n)$ (open triangle) excitation functions for ^{7}Li +^{64}Ni. The 1DBPM and CC predictions are shown by dotted and solid lines, respectively. The PACE prediction for $\sigma_{2n+3n}^{\rm stat}$ is shown by the dashed line.

The resultant excitation function of the extracted $\sigma_{\rm CF}$ is plotted (solid circles) in Fig. 5.

C. Model calculation

To interpret the experimental data of the fusion (TF and CF) excitation functions for the system ^{7}Li +^{64}Ni, the coupled-channels (CC) calculation has been performed using modified version of the code CCFULL [24]. In this version of the code coupling to both the projectile and the target excited states has been incorporated. The Akyüz-Winther potential [25] with the Woods-Saxon parameterization form has been used. The potential parameters are slightly modified to get rid of the oscillation of the fusion excitation function at higher energies. The starting and the modified potential parameters as well as the corresponding uncoupled barrier parameters are given in Table III. The fusion excitation function in the no-coupling condition is used as the 1DBPM excitation function. To understand the effect of deformation of the projectile and the target full CC calculation is done by incorporating first excited states of the projectile and the target. In the CC calculation the first excited state of ^{7}Li ($J^{\pi} = 1/2^{-}$, $E^{*} = 0.478$ MeV), with $B(E2) \uparrow = 7.59\ e^{2}$ fm^{4} [26], has been considered. Also, the reorientation terms for the ground $(3/2^{-})$ and the first excited states are included in the coupling scheme using the ground-state quadrupole moment value of 4.06 fm^{2} [26]. The first

TABLE III. Input potential parameters used in CCFULL calculations along with the resultant barrier parameters.

Potential	V_0 (MeV)	r_0 (fm)	a (fm)	V_B (MeV)	R_B (fm)	$\hbar\omega$ (MeV)
AW	42.1	1.17	0.606	12.20	9.25	3.56
CC	48.0	1.12	0.66	12.20	9.19	3.41

excited state of the target ^{64}Ni ($J^{\pi} = 2^{+}$, $E^{*} = 1.345$ MeV) with deformation $\beta_2 = 0.169$ [27] has also been incorporated in the calculation. The breakup or transfer coupling channel cannot be included in the calculation. The results are shown in Fig. 5 by solid and dotted lines, respectively. It is to be noted that the 1DBPM prediction reproduces the measured TF cross section in the above-barrier energy range but underpredicts the measured values in the below-barrier region. The coupling to inelastic channels enhances the fusion cross sections in the subbarrier energies with respect to values obtained from 1DBPM predictions, but the model excitation function still underpredicts the extracted CF data in the below-barrier region. The enhancement and suppression with respect to 1DBPM has been further explored by defining the quantity *enhancement factor* in the following section.

D. Enhancement and suppression factor

The enhancement factor, EF, to quantify the enhancement or suppression with respect to 1DBPM has been defined as [12],

$$(EF)_i = \frac{\sigma_i}{\sigma_{\rm 1DBPM}}, \qquad i = {\rm TF, CF, CC, 1DBPM}, \ldots \qquad (4)$$

The enhancement factors for the experimental TF, CF, and theoretical CC predictions are plotted in Fig. 6. It is clear that the enhancement of TF cross sections is much steeper compared to the enhancement of CF cross sections at the $E_{\rm c.m.}/V_B < 1$ region. Also, $(EF)_{\rm CC}$ fails to describe the enhancements of both these excitation functions in the subbarrier region. Underprediction of CF cross sections indicates that unlike the case of ^{6}Li, coupling to inelastic excitations alone does not describe the enhancement of CF in the below-barrier region for ^{7}Li + ^{64}Ni. In the above-barrier region $(EF)_{\rm CF}$ is suppressed compared to both $(EF)_{\rm CC}$ and $(EF)_{\rm TF}$, although the effect is not so prominent like the enhancement in the below-barrier energies. The estimated average suppression of $(EF)_{\rm CF}$ (or $\sigma_{\rm CF}$) to $(EF)_{\rm TF}$ (or $\sigma_{\rm TF}$) in the above-barrier region is $6.5 \pm 0.4\%$. However, $(EF)_{\rm CC}$ and $(EF)_{\rm TF}$ matched nicely in this energy region.

To further investigate the origin of the enhancement of TF cross sections in the below-barrier energy regime, two more enhancement factors corresponding to ^{65}Cu and ^{66}Cu residues as a function of energy have been plotted in Fig. 6. As discussed in Sec. III A, both these residues can be populated by CF, ICF, and transfer reactions. Despite their mixed origins, the enhancement profiles of these two residues are significantly different in the below-barrier region. The $(EF)_{66}$, the enhancement factor for ^{66}Cu, increases in the energy region below the barrier compared to its values above it; on the other hand, the $(EF)_{65}$, the enhancement factor for ^{65}Cu, decreases with energy in the same energy range. Apart from the CF process, both these residues can be produced by t-ICF reactions. But distinctly different energy dependencies of the enhancement factors of the two residues probably indicate the dominant contributions of different reaction processes in each case. Therefore, it may be conjectured from the increasing trend of $(EF)_{66}$ that the direct cluster transfer of tritons is primarily responsible for the enhancement of ^{66}Cu cross sections, which in turn causes the enhancement in $\sigma_{\rm TF}$ values at subbarrier energies.

To elaborate this conjecture, we have plotted in Fig. 7 the ratio of the population of individual residues ^{65}Cu and ^{66}Cu through non-CF processes as a function of $E_{\rm c.m.}/V_B$. The population of these residues from CF has been estimated by multiplying experimental $\sigma_{\rm CF}$ with corresponding branching ratios obtained from SM calculations. The non-CF contribution of each residue is subsequently determined by subtracting the extracted cross section of the CF component from the measured cross section of each residue. The ratios of non-CF

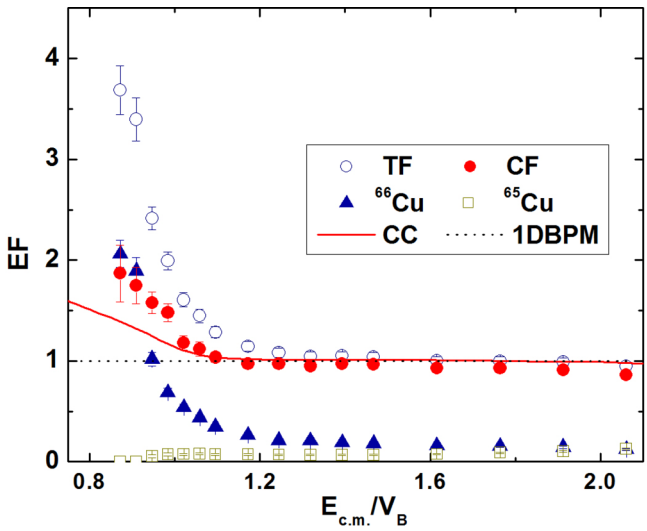

FIG. 6. The enhancement factors of TF, CF, and CC cross sections relative to the 1DBPM cross sections are plotted as a function of $E_{\rm c.m.}/V_B$, where V_B is the height of the fusion barrier from Table III. The same for the residue channels ^{65}Cu and ^{66}Cu are also shown by open boxes and solid triangles, respectively.

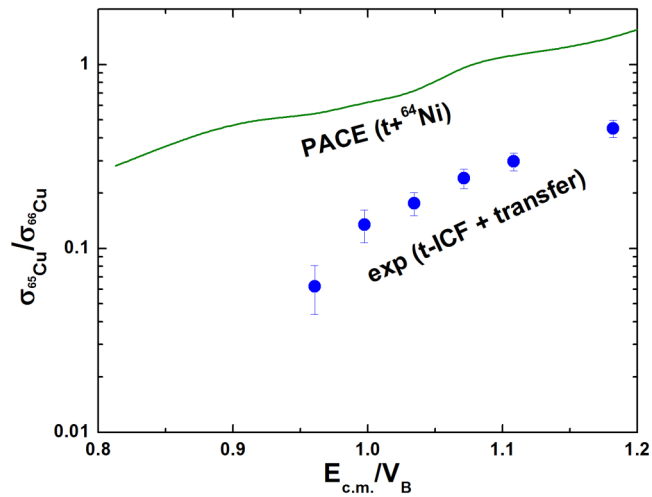

FIG. 7. Ratio of the non-CF cross sections for the residues ^{65}Cu and ^{66}Cu for the system ^{7}Li + ^{64}Ni. The solid bullets represent the data and the solid line represents the calculation from the SM model. See text for details.

cross sections for ^{65}Cu and ^{66}Cu are shown by solid bullets in Fig. 7.

The theoretical curve shown in the figure is generated from the ratio of ^{65}Cu and ^{66}Cu cross sections from the fusion of ^{3}H (t) moving with the beam velocity of ^{7}Li, with ^{64}Ni target. This ratio should reflect the ratio of cross sections of these two channels produced through the t-ICF process. The large mismatch between the experimental and theoretical curves indicates again a high yield of residue ^{66}Cu from reactions other than t-ICF at subbarrier energies. The other reaction modes in producing ^{66}Cu are d- or t-stripping reactions from ^{7}Li. From Q-value and spectroscopic arguments, one can conclude that triton transfer from ^{7}Li is the most dominant channel in this energy regime. Also vanishingly small cross sections of ^{65}Cu at subbarrier energies show that one-proton stripping does not have significant contribution at the subbarrier energies.

IV. COMPARISON WITH ^{6}Li + ^{64}Ni

We have compared the present experimental results with previously measured results of ^{6}Li + ^{64}Ni. The ratio of the measured TF cross sections of ^{6}Li and ^{7}Li with ^{64}Ni is plotted with respect to $E_{\mathrm{c.m.}}/V_B$ in Fig. 8, in comparison with other low-mass-target systems. The data for fusion cross sections of other low-mass-target systems and the corresponding Coulomb barrier values, V_B, have been taken from Refs. [11,14,15]. The figure shows that in the above-barrier region the ratio is nearly unity, but as energy decreases it exhibits a rising trend for all the systems. Our experimental observation also corroborates with the systematic trend. With data existing in small energy steps in the present measurement, the upward bend in the ratio just below $E_{\mathrm{c.m.}}/V_B = 1$ is very clearly observed. Also in the below $E_{\mathrm{c.m.}}/V_B \sim 1$ region, the $\sigma(^{6}\mathrm{Li})/\sigma(^{7}\mathrm{Li})$ ratio for the ^{64}Ni target matches quite nicely with the same ratio for the ^{64}Zn target [11] although the

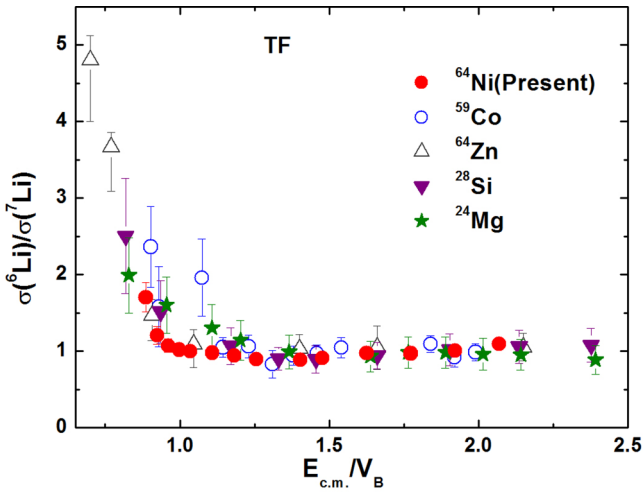

FIG. 8. Ratio of ^{6}Li to ^{7}Li TF cross sections as a function of the *reduced* center-of-mass energy. The ratio with the ^{64}Ni target (solid bullets) is compared with the same ratio with other medium- and low-mass targets taken from Refs. [11,14]. See text for details.

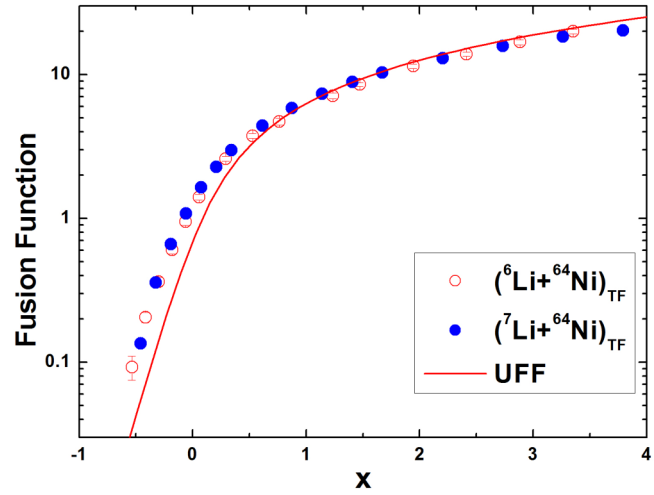

FIG. 9. Experimental reduced TF cross section for the systems ^{6,7}Li + ^{64}Ni. The solid line represents the UFF. For details, see the text.

measurement in the present experiment does not extend to energies well below the barrier. In probing the origin of the behavior, CC calculations within the CDCC framework for the systems ^{6,7}Li + ^{59}Co [13,28] have been performed and the conclusion is that the observed rising trend in the cross section ratio is due to the difference in breakup thresholds of the two projectiles. Further, in a systematic analysis of ^{6,7}Li + ^{64}Zn TF data [11], the authors conjectured that the upward rise in the ratio of ^{6,7}Li fuison cross sections is observed because of the dominance of ICF and/or DCT or of single nucleon transfer reactions in the subbarrier energy region for the projectile ^{6}Li over ^{7}Li, although clear separation of the ICF and/or the DCT reactions from the measured fusion data for ^{6,7}Li fusion could not be achieved.

To further compare the outcome of fusion of ^{6}Li and ^{7}Li with the ^{64}Ni target, we constructed the dimensionless quantities, fusion function $F(x)$ and x, as

$$F(x) = \frac{2E_{\mathrm{c.m.}}}{R_B^2 \hbar\omega}\sigma_F, \quad x = \frac{E_{\mathrm{c.m.}} - V_B}{\hbar\omega}, \tag{5}$$

with the measured σ_{TF} and σ_{CF} cross sections following the prescription of Canto *et al.* [29]. The barrier parameters used in the expressions are taken from our 1DBPM calculations for ^{6,7}Li + ^{64}Ni systems. By construction, the fusion function $F(x)$ takes care of the static effects of the barrier properties of the systems and hence any difference in $F(x)$ between the two systems should reflect the difference in the dynamic effect due to the reactions like breakup or transfer.

We constructed the $F(x)$ functions with the measured σ_{TF} of ^{6}Li + ^{64}Ni and ^{7}Li + ^{64}Ni systems and plotted them with respect to x in Fig. 9. The functions are compared with the universal fusion function (UFF), $F_0(x) = \ln[1 + \exp(2\pi x)]$ of variable x, in the plot. Enhancement in $F(x)$ compared to $F_0(x)$ for both the systems has been observed in the subbarrier energy region. Interestingly, the enhancements are same for both ^{6}Li and ^{7}Li projectiles. This indicates that the origin of

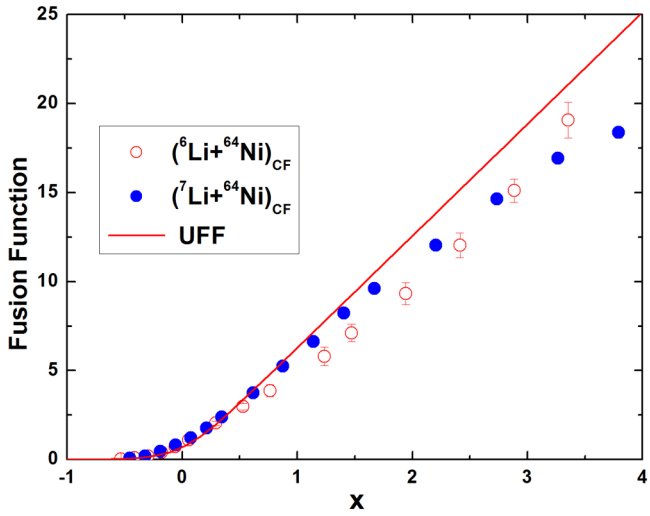

FIG. 10. Experimental reduced CF cross section for the systems ^{6,7}Li + ^{64}Ni. The solid line represents the UFF. For details, see the text.

enhancement of the total fusion cross section below the barrier is not due to the breakup coupling.

In Fig. 10, fusion functions $F(x)$, constructed with the extracted CF cross sections, σ_{CF}, of the two systems, have been shown in comparison with the universal fusion function $F_0(x)$. The fusion functions of the ^{6}Li + ^{64}Ni and ^{7}Li + ^{64}Ni systems differ in the above-barrier region. The function corresponding to ^{6}Li + ^{64}Ni shows greater suppression relative to $F_0(x)$ in comparison to that for ^{7}Li + ^{64}Ni at above-barrier energies. In the below-barrier region, the fusion functions with σ_{CF} for both the systems overlap nicely with the universal fusion function. Thus unlike the above-barrier energies where the breakup affects the complete fusion of the two projectiles differently, the complete fusion cross sections of the projectiles are unaffected by any dynamical process present in the subbarrier energy region.

V. SUMMARY AND CONCLUSION

The measurement of total fusion cross sections at near-barrier energies as a function of incident energy for the system ^{7}Li + ^{64}Ni has been presented in the present article. The fusion excitation function has been determined from the online detection of characteristic γ rays from the residues. Using the measured cross sections of the dominant $2n$- and $3n$-decay channels of the compound nucleus ^{71}Ga and obtaining the branching ratio for the summed ($2n$ and $3n$)-channel cross section to the pure complete fusion cross section from statistical model calculations, the experimental CF cross sections have been obtained at each energy. An offline detection of the delayed x ray of Zn produced from electron capture in ^{68}Ga, the $3n$-channel residue formed in the fusion of ^{7}Li and ^{64}Ni at 26 MeV, has been performed. Unstable ^{68}Ga with $T_{1/2} = 67.7$ min is produced only in the complete fusion process. Reasonably good matching of the offline and online measurements corroborates the earlier observation that direct ground-state feeding in this mass region is not significant.

Comparison of the extracted CF cross sections at above-barrier energies shows that the average suppression in the ^{7}Li + ^{64}Ni system is ~6.5%, a value lower than that for the ^{6}Li + ^{64}Ni system (~13%). The difference in the suppression between the two stable isotopes of Li is clearly visible in the comparison with the *universal fusion function* that brings out the dynamic effect of breakup or breakup-like processes in the above-barrier energies. The degree of suppression is also much less compared to fusion of ^{7}Li with the heavy targets like ^{209}Bi [3], ^{159}Tb [7], and ^{144}Sm [8], where the observed suppression is of the order of 25%.

In the below-barrier energy region, both TF and CF cross sections of the ^{7}Li + ^{64}Ni system are enhanced with respect to 1DBPM predictions. The enhancement in TF is much sharper than the enhancement in CF. However, unlike ^{6}Li + ^{64}Ni, the CF enhancement for ^{7}Li + ^{64}Ni could not be explained by coupling to inelastic channels only, indicating the presence of possible coupling to transfer reaction channels for ^{7}Li in the below-barrier region. Extension of measurement to still subbarrier energies and subsequent coupled-channels analysis including the transfer degree of freedom is needed to clarify the observation.

ACKNOWLEDGMENTS

We sincerely thank the Pelletron staff for providing a steady and uninterrupted ^{7}Li beam. We would also like to thank Mr. S. Biswas and Mr. Kiran Divekar of DNAP, TIFR, for their support during the experiment. One of the authors, Md.M.S. would like to thank the Council of Scientific & Industrial Research, India, for their financial support.

[1] L. F. Canto, P. R. S. Gomes, R. Donangelo, and M. S. Hussein, Phys. Rep. **424**, 1 (2006).
[2] B. B. Back, H. Esbensen, C. L. Jiang, and K. E. Rehm, Rev. Mod. Phys. **86**, 317 (2014).
[3] M. Dasgupta, D. J. Hinde, K. Hagino, S. B. Moraes, P. R. S. Gomes, R. M. Anjos, R. D. Butt, A. C. Berriman, N. Carlin, C. R. Morton, J. O. Newton, and A. Szanto de Toledo, Phys. Rev. C **66**, 041602(R) (2002).
[4] M. Dasgupta, P. R. S. Gomes, D. J. Hinde, S. B. Moraes, R. M. Anjos, A. C. Berriman, R. D. Butt, N. Carlin, J. Lubian, C. R. Morton, J. O. Newton, and A. Szanto de Toledo, Phys. Rev. C **70**, 024606 (2004).
[5] C. S. Palshetkar, Shital Thakur, V. Nanal, A. Shrivastava, N. Dokania, V. Singh, V. V. Parkar, P. C. Rout, R. Palit, R. G. Pillay, S. Bhattacharyya, A. Chatterjee, S. Santra, K. Ramachandran, and N. L. Singh, Phys. Rev. C **89**, 024607 (2014).
[6] Vandana Tripathi, A. Navin, K. Mahata, K. Ramachandran, A. Chatterjee, and S. Kailas, Phys. Rev. Lett. **88**, 172701 (2002).
[7] A. Mukherjee, Subinit Roy, M. K. Pradhan, M. Saha Sarkar, P. Basu, B. Dasmahapatra, T. Bhattacharya, S. Bhattacharya, S. K.

Basu, A. Chatterjee, V. Tripathi, and S. Kailas, Phys. Lett. B **636**, 91 (2006).
[8] P. K. Rath, S. Santra, N. L. Singh, B. K. Nayak, K. Mahata, R. Palit, K. Ramachandran, S. K. Pandit, A. Parihari, A. Pal, S. Appannababu, Sushil K. Sharma, D. Patel, and S. Kailas, Phys. Rev. C **88**, 044617 (2013).
[9] D. J. Hinde, M. Dasgupta, B. R. Fulton, C. R. Morton, R. J. Wooliscroft, A. C. Berriman, and K. Hagino, Phys. Rev. Lett. **89**, 272701 (2002).
[10] P. R. S. Gomes, I. Marti, M. D. Rodríguez, G. V. Martí, R. M. Anjos, J. Lubian, R. Veiga, R. Liguori Neto, E. Crema, N. Added, L. C. Chamon, J. O. Fernández Niello, O. A. Capurro, A. J. Pacheco, J. E. Testoni, D. Abriola, A. Arazi, M. Ramírez, and M. S. Hussein, Phys. Lett. B **601**, 20 (2004).
[11] A. Di Pietro, P. Figuera, E. Strano, M. Fisichella, O. Goryunov, M. Lattuada, C. Maiolino, C. Marchetta, M. Milin, A. Musumarra, V. Ostashko, M. G. Pellegriti, V. Privitera, G. Randisi, L. Romano, D. Santonocito, V. Scuderi, D. Torresi, and M. Zadro, Phys. Rev. C **87**, 064614 (2013).
[12] Md. Moin Shaikh, Subinit Roy, S. Rajbanshi, M. K. Pradhan, A. Mukherjee, P. Basu, S. Pal, V. Nanal, R. G. Pillay, and A. Shrivastava, Phys. Rev. C **90**, 024615 (2014).
[13] C. Beck *et al.*, Phys. Rev. C **67**, 054602 (2003).
[14] Mandira Sinha, H. Majumdar, P. Basu, Subinit Roy, R. Bhattacharya, M. Biswas, M. K. Pradhan, R. Palit, I. Mazumdar, and S. Kailas, Eur. Phys. J. A **44**, 403 (2010).
[15] M. Ray, A. Mukherjee, M. K. Pradhan, Ritesh Kshetri, M. Saha Sarkar, R. Palit, I. Majumdar, P. K. Joshi, H. C. Jain, and B. Dasmahapatra, Phys. Rev. C **78**, 064617 (2008).
[16] A. Mukherjee, U. Datta Pramanik, S. Chattopadhyay, M. Saha Sarkar, A. Goswami, P. Basu, S. Bhattacharya, M. L. Chatterjee, and B. Dasmahapatra, Nucl. Phys. A **645**, 13 (1999).
[17] Computer code LAMPS (Linux Advanced Multiparameter System), http://www.tifr.res.in/∼pell/lamps.html.
[18] http://www.nndc.bnl.gov.in/nudat2.
[19] E. B. Shera and H. H. Bolotin, Phys. Rev. **169**, 940 (1968).
[20] S. I. Salem, S. L. Panossian, and R. A. Krause, At. Data Nucl. Data Tables **14**, 91 (1974).
[21] S. Cavallaro, L. Y. Xiao, M. L. Sperduto, and J. Delaunay, Nucl. Instrum. Methods Phys. Res., Sect. A **245**, 89 (1986).
[22] P. R. S. Gomes, T. J. P. Penna, R. Liguori Neto, J. C. Acquadro, C. Teneiro, E. Crema, N. Carlin Filho, and M. M. Coimbra, Nucl. Instrum. Methods Phys. Res., Sect. A **280**, 395 (1989).
[23] A. Gavron, Phys. Rev. C **21**, 230 (1980).
[24] K. Hagino, N. Rowley, and A. T. Kruppa, Comput. Phys. Commun. **123**, 143 (1999).
[25] O. Akyüz and A. Winther, *Proceedings of the International School of Physics "Enrico Fermi,"* Course LXXVII, edited by R. A. Broglia, R. A. Ricci, and C. H. Dasso (North-Holland, Amsterdam, 1981), p. 492.
[26] W. J. Vermeer, R. H. Spear, and F. C. Barker, Nucl. Phys. A **500**, 212 (1989).
[27] B. Pritychenko, M. Birch, B. Singh, and M. Horoi, At. Data Nucl. Data Tables **107**, 1 (2016).
[28] A. Diaz-Torres, I. J. Thompson, and C. Beck, Phys. Rev. C **68**, 044607 (2003).
[29] L. F. Canto, P. R. S. Gomes, J. Lubian, L. C. Chamon, and E. Crema, Nucl. Phys. A **821**, 51 (2009).